Kuhlmann, J., Dobslaw, H., Thomas, M. (2011): Improved modelling of sea-level patterns by incorporating self-attraction and loading. - Journal of Geophysical Research, 116, C11036

DOI: 10.1029/2011JC007399

Improved modeling of sea level patterns by incorporating self-attraction and loading

J. Kuhlmann,[1,2] H. Dobslaw,[1] and M. Thomas[1,2]

Received 21 June 2011; revised 8 September 2011; accepted 13 September 2011; published 23 November 2011.

[1] We implement the effects of gravitational self-attraction and loading (SAL) into a global baroclinic ocean circulation model and investigate effects on sea level patterns, ocean circulation, and density distributions. We compute SAL modifications as an additional force on the water masses at every time step by decomposing the field of ocean bottom pressure anomalies into spherical harmonic functions and then applying Love numbers to account for the elastic properties of the solid Earth. Considering SAL in the postprocessing turns out to be insufficient, especially in coastal waters and on subweekly time scales, where SAL modifies local sea level by around 0.6–0.8 cm on average; in the open ocean, changes mostly remain around 0.3 cm. Modifications of water velocities as well as of heat and salt distributions are modeled, yet they are small. Simple parameterizations of SAL effects currently used in a number of ocean circulation models suffer from the process's inhomogeneity in space and time. These parameterizations improve the modeled sea level patterns but fail to reproduce SAL impacts on circulation and density distributions. We therefore suggest to explicitly consider the full SAL effect in ocean circulation models, especially when investigating sea level variations faster than around 4 days.

Citation: Kuhlmann, J., H. Dobslaw, and M. Thomas (2011), Improved modeling of sea level patterns by incorporating self-attraction and loading, *J. Geophys. Res.*, *116*, C11036, doi:10.1029/2011JC007399.

1. Introduction

[2] While global sea level has been rising since the onset of the industrialization [*Church and White*, 2006; *Cazenave et al.*, 2009], regional sea level shows far more variable patterns on multiple scales in space and time [e.g., *Thompson and Demirov*, 2006; *Wunsch et al.*, 2007; *Oliver and Thompson*, 2010]. Such patterns are caused by changes in water temperature and salinity, ocean circulation, atmospheric surface pressure, and deformations of the solid Earth and the geoid [*Bindoff et al.*, 2007]. Successively, these effects are being implemented into numerical ocean general circulation models (OGCMs). Yet, considerable uncertainties in sea level projections remain. For instance, the intermodel standard deviation of local secular sea level trends exceeds the magnitude of those patterns in large parts of the ocean [*Meehl et al.*, 2007; *Yin et al.*, 2010]. Improving the representation of those physical effects influencing sea level patterns in OGCMs is therefore highly relevant for a better simulation of this scientifically and societally crucial variable.

[3] The effects of gravitational self-attraction and loading (SAL), for instance, are either oversimplifyingly parameterized or even outrightly ignored in many OGCMs. The reason for omitting this well-understood effect is the high cost in terms of computing time. SAL has first been described in the early 1970s [*Farrell*, 1973]. Its complete treatment requires either a decomposition into spherical harmonic functions or a convolution of the field of ocean bottom pressure anomalies (p'_B), with both ways being equally demanding in terms of computing time. For tidal models, a simple parameterization that goes back to the work of *Accad and Pekeris* [1978] avoids those kinds of calculations. It consists in simply multiplying the p'_B field by a constant factor. This approach is justified if one spatial scale is dominant in the p'_B field, which was thought to be valid for tides. In view of the rapidly improving accuracy of global geodetic observations, *Ray* [1998] already showed in the late 1990s for tidal models that such a scalar approximation introduces large errors, leading him to the conclusion that "it is difficult to imagine any geodetic application sufficiently precise to warrant ocean-loading corrections and yet sufficiently imprecise to warrant the scalar approximations." Because of the multitude of processes and therefore spatial scales in the general circulation, the prospects of a scalar approximation in OGCMs are even more dire.

[4] On that account, there have been various attempts by ocean modelers to consider SAL in more sophisticated ways: *Stepanov and Hughes* [2004] implemented SAL with a convolution approach into a barotropic OGCM, focusing on short time scales, *Vinogradova et al.* [2010, 2011] investigated SAL on monthly and longer time scales, com-

[1]Section 1.3: Earth System Modelling, GFZ German Research Centre for Geosciences, Potsdam, Germany.
[2]Institute of Meteorology, Freie Universität Berlin, Berlin, Germany.

0148-0227/11/2011JC007399

puting the effects as a correction to the model output (a method henceforth called offline calculation), and *Tamisiea et al.* [2010] used the same approach, comparing SAL to similar effects caused by land hydrology and atmospheric loading with a focus on the annual cycle. One limitation of these earlier works is that they fail to allow for dynamic responses of the ocean circulation. An altered ocean circulation may lead to a redistribution of heat and salt which in turn modifies sea level patterns. This can only be achieved by computing SAL effects during the integration of the OGCM (henceforth called online calculation). To our knowledge, we provide the first attempt to run a baroclinic OGCM in a configuration allowing for these effects.

[5] Questions we will answer are: Of what magnitude are SAL effects on relative sea level, ocean circulation, and water density? How useful is an offline calculation of SAL? Does it make sense to treat SAL with a scalar approximation? And how large are our errors if we do so?

2. The Ocean Model for Circulation and Tides Model

[6] The OGCM we use for this study is the Ocean Model for Circulation and Tides (OMCT) [*Thomas*, 2002]. The OMCT is a direct descendant of the Hamburg Ocean Primitive Equation Model [*Wolff et al.*, 1996; *Drijfhout et al.*, 1996], but it has been optimized for shorter time scales and can simulate tides as well. It is a serial model based on the nonlinear momentum balance equation, the continuity equation, and conservation equations for heat and salt. The Boussinesq approximation is applied, and the total ocean mass is held constant at every time step following the work by *Greatbatch* [1994]. The OMCT in the current configuration has a regular grid of 1.875° resolution in both latitude and longitude. Vertically, the model ocean is discretized at 13 layers whose thicknesses increase with depth but are constant in time. Each model time step is 30 min long. The OMCT has first reached a quasi steady state circulation in a spin-up simulation with climatological wind stresses and mean sea surface temperatures and salinities. Subsequently, it is driven by 6-hourly wind stresses, atmospheric surface pressure, 2 m temperatures, and freshwater fluxes due to precipitation and evaporation. All of these forcing fields are provided by the ERA-Interim reanalysis project [*Dee et al.*, 2011] of the European Centre for Medium-Range Weather Forecast (ECMWF). Additionally, forcing from continental runoff, excluding ice sheet contributions, was obtained from the Land Surface Discharge Model (LSDM) [*Dill*, 2008] which is based on ERA-Interim reanalysis data as well. In this study, we analyze 6-hourly output of a simulation in which tidal forcing was deactivated. The study period is the year 2008.

[7] The OMCT has recently been used for investigations of the Earth's rotational parameters [*Dobslaw et al.*, 2010] and routinely helps to dealias GRACE satellite data [*Flechtner*, 2007]. *Quinn and Ponte* [2011] showed that the general agreement of OMCT's p'_B signals with in situ data on time scales shorter than 60 days is relatively weak. Still, in terms of high-frequency p'_B variance, OMCT turned out to come closer to observations than other models, which the authors explained with the inclusion of atmospheric pressure loading in OMCT. In another study, *Chambers and Willis* [2010] compared monthly p'_B fields from OMCT with altimetric data that they had corrected for steric effects with the help of data from the Argo float network. In this comparison, OMCT achieved high correlations with the observational data almost globally, while some discrepancies appeared in the Southern Ocean.

3. Implementation of Self-Attraction and Loading

[8] We derive the magnitude of the combined effects due to self-attraction and loading (SAL) for a baroclinic ocean. The barotropic case has been dealt with by *Ray* [1998] and *Müller* [2007].

3.1. The Self-Attraction Part

[9] The gravitational potential at a location **p** induced by a point mass m located at **q** in its most general form is

$$V(\mathbf{p}) = \gamma \frac{m}{\overline{\mathbf{pq}}} \tag{1}$$

with γ being the gravitational constant. We make the assumption that, since the ocean depth is at least 1000 times smaller than the Earth's radius, we can approximate the ocean as an infinitely thin spherical shell. For such a shell, equation (1) turns into

$$V(\mathbf{p}) = \gamma \int\int_S \frac{\sigma(\mathbf{q})}{\overline{\mathbf{pq}}} dS. \tag{2}$$

Here $\sigma(\mathbf{q})$ is the surface mass density, i.e., the mass per unit area, at location **q** and the integration is carried out over the entire spherical layer. When Ω is the solid angle between **p** and **q** and R the sphere's radius, the distance between the two points on the sphere is [*Abramowitz and Stegun*, 1972, p. 72]

$$\overline{\mathbf{pq}} = 2R \sin\left(\frac{\Omega}{2}\right) = 2R\sqrt{\frac{1-\cos\Omega}{2}} = R\sqrt{2-2\cos\Omega}, \tag{3}$$

which resembles the series of the Legendre Polynomials

$$\sum_{n=0}^{\infty} P_n(\cos\Omega) = \frac{1}{\sqrt{2-2\cos\Omega}} = \frac{R}{\overline{\mathbf{pq}}}. \tag{4}$$

Now let us insert this into equation (2), considering that since we are on a spherical shell of zero thickness, the surface mass density $\sigma(\mathbf{q})$ is $\sigma(\lambda', \varphi')$

$$V(\mathbf{p}) = \frac{\gamma}{R} \int\int_S \sigma(\lambda', \phi') \sum_{n=0}^{\infty} P_n(\cos\Omega) dS \tag{5}$$

We know that we can decompose our surface mass density into spherical harmonics as

$$\sigma_n(\lambda, \phi) = \frac{2n+1}{4\pi R^2} \int\int_S \sigma(\lambda', \phi') P_n(\cos\Omega) dS. \tag{6}$$

This holds for a spherical shell of radius R (see *Smirnow* [1955, p. 427] for a description of the special case $R = 1$). Note that σ_n includes a summation over all orders $m = 0, \ldots, n$, which we omitted here for brevity. Back to equation (5): We exchange the integration and the summation, which we can do since $\sigma(\lambda', \varphi')$ does not depend on n, and we then

replace the integral with the identical expression from equation (6). This leads us to

$$V(\mathbf{p}) = \gamma 4\pi R \sum_{n=0}^{\infty} \frac{\sigma_n(\lambda,\phi)}{2n+1}. \quad (7)$$

Rewriting the gravitational constant γ in terms of Earth's gravity g leads us to a new expression for the potential of our spherical shell:

$$V(\mathbf{p}) = \frac{4\pi R^3 g}{M_e} \sum_{n=0}^{\infty} \frac{\sigma_n(\lambda,\phi)}{2n+1}. \quad (8)$$

We clean up a little by inserting the average density of the Earth $\rho_e = 3M_e/(4\pi R^3)$

$$V(\mathbf{p}) = \frac{3g}{\rho_e} \sum_{n=0}^{\infty} \frac{\sigma_n(\lambda,\phi)}{2n+1}. \quad (9)$$

Since we wish to express our surface mass density in terms of bottom pressure anomalies p'_B, we make use of the relation $p = \rho g h$: Our surface mass density σ_n equals volume density ρ times the vertical dimension h, so we replace it with $p'_{B,n}/g$, which leads to

$$V(\mathbf{p}) = \frac{3}{\rho_e} \sum_{n=0}^{\infty} \frac{p'_{B,n}(\lambda,\phi)}{2n+1}. \quad (10)$$

This is the additional potential on a water parcel at location $\mathbf{p}$ due to gravitational attraction by the anomalous mass distribution on the spherical shell that is described by the spherical harmonics $p'_{B,n}$.

3.2. The Loading Part

[10] SAL consists of three separate effects, the first of them being the gravitational attraction we just described. What about loading? It leads to the other two SAL effects. On the one hand, the additional mass lowers the seafloor, deforming the Earth elastically; the amount of this displacement is $h'_n\ V_n/g$, which defines the load Love numbers h'_n. On the other hand, the elastic redistribution of Earth masses in response to the loading shifts the gravitational potential by an amount of $k'_n\ V_n/g$; again, this defines the load Love numbers k'_n [*Munk and MacDonald*, 1960, p. 24]. The loading effects are thus proportional to the additional mass, with the proportionality factors reflecting the solid Earth's properties.

[11] The combination of these three effects that an additional mass exerts (self-attraction, seafloor lowering, and inner Earth mass redistribution) requires us to multiply the additional potential from equation (10) with a factor $(1 + k'_n - h'_n)$. This holds for calculations at points fixed relative to the seafloor, thus for a Lagrangian observer [e.g., *Blewitt*, 2007, p. 385]. This Lagrangian point of view is most convenient for us: It saves us from having to redefine the positions of our grid points and to manipulate our layer thicknesses at every time step, but it still allows us to consider the dynamical effects of a moving seabed.

3.3. Implementation Into the Model

[12] The point in our model where we want to implement SAL effects is the computation of horizontal velocities due to pressure gradients since forces from an additional potential take the same analytical form. The volume force on a water parcel is the negative gradient of the pressure field,

$$\mathbf{F}_{Vol} = -\mathrm{grad}p. \quad (11)$$

We seek to obtain an equivalent formulation for the volume force due to the gravitational potential $\Delta\mathbf{F}_{Vol}$, so we consider that the gradient of the potential is the acceleration, the acceleration times the mass is the force, and the force divided by the volume is the volume force,

$$\Delta\mathbf{F}_{Vol} = \frac{m}{Vol}\mathrm{grad}V = \rho\mathrm{grad}V. \quad (12)$$

Hence, in places where the numerical model calculates volume forces from the pressure field, we can modify the local volume force with the product of the local water density and the gradient of an additional potential. The modified potential in turn is computed from ocean bottom pressure anomalies with respect to an annual mean field.

[13] We can finally express the modification of local horizontal forces on a water parcel due to SAL as

$$\Delta\mathbf{F}_{Vol} = \rho(\mathbf{p})\mathrm{grad}\left(\sum_{n=0}^{\infty}(1 + k'_n - h'_n)\alpha'_n p'_{B,n}(\mathbf{p})\right) \quad (13)$$

with

$$\alpha'_n = \frac{3}{\rho_e(2n+1)}.$$

[14] For our numerical experiments, we perform three different runs with the OMCT ocean model, hereafter called Love, beta0.1, and noSAL. We use the formulation from equation (13) for the Love model run. Herein, we use the Spherepack 3.2 routine (J. C. Adams and P. N. Swarztrauber, SPHEREPACK 3.2: A model development facility, 2009, available at http://www.cisl.ucar.edu/css/software/spherepack/) for the decomposition of p'_B into spherical harmonics up to degree and order 97, thereby making optimal use of the model's horizontal resolution. We obtained a set of load Love numbers based on the PREM Earth model [*Dziewonski and Anderson*, 1981] from http://gemini.gsfc.nasa.gov/agra/.

[15] The aforementioned scalar approximation first proposed by *Accad and Pekeris* [1978] consists in omitting the degree dependence of the Love numbers. This is justified when the terms of one certain degree dominate the sum of the Stokes coefficients $p'_{B,n}$. Then, equation (13) simplifies to

$$\begin{aligned}\Delta\mathbf{F}_{Vol} &= \rho(\mathbf{p})\mathrm{grad}\left(\sum_{n=0}^{\infty}\beta p'_{B,n}(\mathbf{p})\right) \\ &= \rho(\mathbf{p})\beta\mathrm{grad}p'_B(\mathbf{p}),\end{aligned} \quad (14)$$

making the decomposition into spherical harmonics unnecessary. We apply this formulation in the beta0.1 model run.

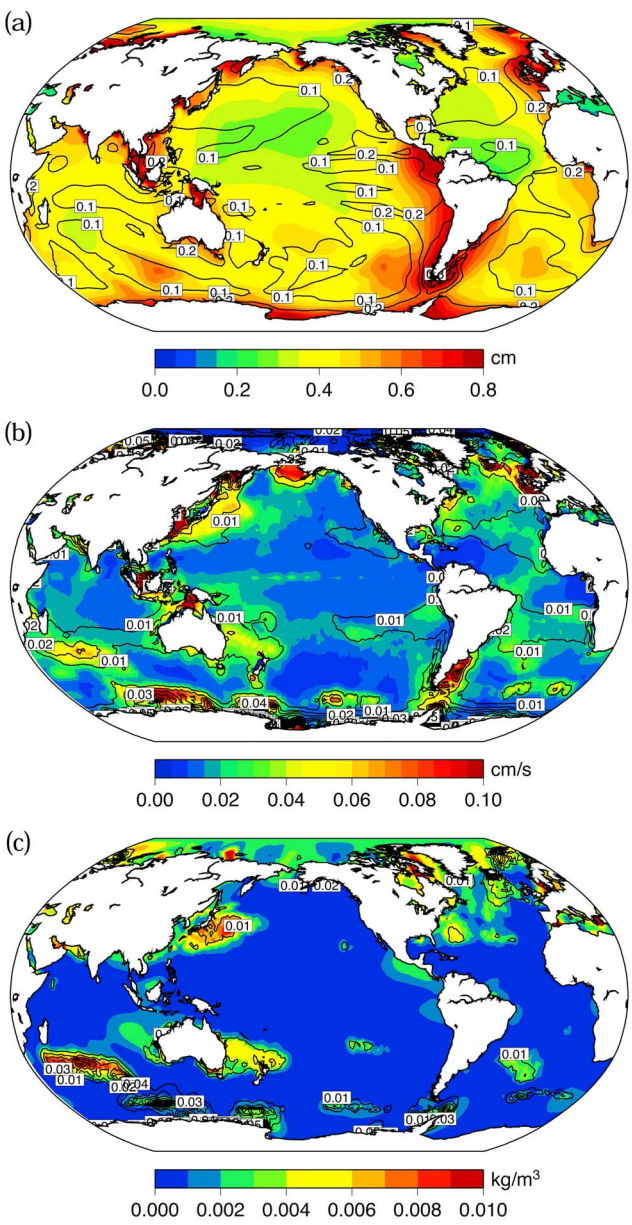

Figure 1. Anomalies in (a) relative sea level, (b) absolute horizontal velocity in the upper 90 m, and (c) water density in the upper 90 m caused by self-attraction and loading (SAL) effects. Colors show the absolute impact of SAL effects in terms of the standard deviation of differences between the Love run and the noSAL run. Black contour lines show the relative impact of SAL effects in terms of the former quantity divided by the standard deviation of the Love run.

[16] For the control run noSAL, we set $\Delta \mathbf{F}_{Vol} \equiv 0$, thereby neglecting all SAL effects.

4. Results

[17] In order to judge how significant the modifications by appropriately modeled SAL effects on different variables are, we show in Figure 1 the standard deviation of differences between the Love run and the noSAL run, thus the root-mean square differences between the two runs or, equally, the anomalies caused by SAL. We choose to show these differences for the sea level relative to the ocean floor (Figure 1a), the absolute horizontal water velocity in the upper 90 m of the ocean (approximately the mixed layer; Figure 1b), and the water density modified by temperature and salinity in the same layer (Figure 1c). In Figure 1, we overlay contour lines that display this standard deviation of differences divided by the standard deviation of the Love run alone, i.e., σ(Love − noSAL)/σ(Love). This quantity is to give an impression of SAL's relative importance. The SAL-induced potential acts identically on water in all depths. In the mixed layer, however, horizontal density gradients are largest, so we expect the most pronounced baroclinic effects here.

[18] Figure 1a shows that in absolute values of sea level, SAL is mostly a coastal effect. Here strong and varying currents lead to substantial p_B anomalies that induce SAL. Coastal mean deviations commonly reach 0.6 to 0.8 cm, which is equivalent to more than 10% of the simulated sea level variations in many of those regions. Strong current systems even exert SAL forces on calmer neighboring regions, as evident in the eastern tropical Pacific, where this leads to mean modifications of the sea level by 20% and more. In the open ocean, deviations mostly remain around 0.3 cm, which translates into around 10%.

[19] In terms of absolute horizontal velocity (Figure 1b), SAL is less important. It alters currents by at most 0.1 cm/s, and even this value is only apparent in marginal waters, where simulated velocities are rather inexact because of OMCT's coarse coastline resolution. Horizontal velocities are altered by around 0.05 cm/s in strong current systems such as the Kuroshio, the Gulf Stream, the Antarctic Circumpolar Current (ACC), and the Malvinas Current, where the modifications pale in comparison to the local standard deviations of velocities. The relative SAL impact on mixed-layer velocities therefore mostly remains below 2%.

[20] Changes in ocean currents can lead to changes in the distribution of heat and salt, which in turn can be summarized as density effects. Figure 1c shows these effects. In regions of larger velocity modifications, density anomalies are induced, e.g., in the Gulf Stream, the Kuroshio, and north of the ACC along a latitudinal band centered at 30°S. Here, the modifications reach between 0.005 and 0.010 kg/m^3. Except for parts of the southern Indian Ocean, these deviations imply that a dismissal of SAL effects would result in an error of up to 1% only.

[21] Investigations of the evolution of density modifications in time showed that there is no strong trend in the signal: The impact of SAL on sea level is therefore mostly barotropic. This implies that considering SAL at every model time step is mainly important on short time scales. Slow sea level changes, which are dominated by baroclinic processes, are less affected.

[22] A common approach to SAL is the computation of offline corrections to sea level fields, which, for instance, *Vinogradova et al.* [2010, 2011] and *Tamisiea et al.* [2010] have done for investigations on longer time scales. We check the validity of this approach for our study by correlating the forcing to our SAL routine and the model ocean's response to it. High correlations would indicate a linear

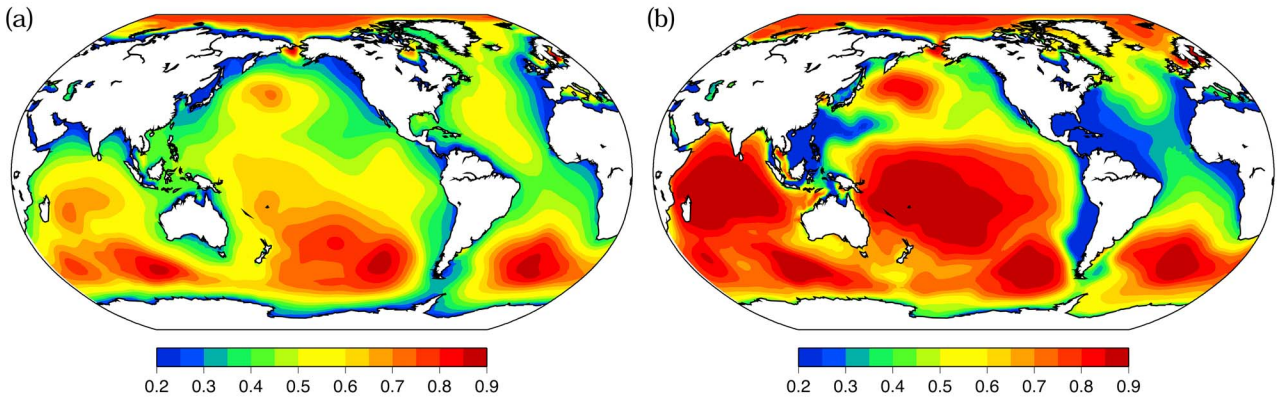

Figure 2. Correlations computed along the time axis for every grid point of two fields describing the SAL forcing and the response. Forcing is the modification to the local potential due to self-attraction and loading (the sum in equation (13)). Response is the difference in sea level between the Love run and the noSAL run, thus the anomalous sea level caused by self-attraction and loading. The correlations were computed from (a) 6-hourly data and (b) weekly means. In Figure 2a, a time lag of +6 h is included, supposedly giving the model ocean enough time to adapt to the changed potential. We have tried different lag times between −12 h and +12 h; the correlations reached a maximum at +6 h, which is the field shown here. In Figure 2b, we did not apply time lags.

response, in which case the offline approach would be sufficient. As forcing term, we take the sum in equation (13), which describes a modification to the local gravitational potential; its gradient acts as a force on the water parcel. As response term, we take the difference in sea level between a run with SAL considered (Love) and a run with SAL switched off (noSAL). Since the model ocean is expected to take a certain time to adapt to the changed potential, we investigate different time lags between forcing and response fields. Possible time lags are restricted by the 6-hourly time resolution of both fields. The maximum correlation is achieved with a time lag of +6 h.

[23] The geographical distribution of these correlations is shown in Figure 2a. The correlation coefficients are always positive, they vary between 0.2 and 0.8. The lowest values are generally found along the coasts, while high values are achieved in the open ocean, especially in the southern hemisphere and in the Arctic Ocean. As expected, values close to the coasts are lower: a coast constitutes a horizontal boundary that limits the area from where inflowing water can balance a change in potential. On the other hand, coastal sea level is especially crucial when it comes to predictions for human populations and ecosystems.

[24] If the sea level response of a model considering SAL is only loosely correlated to the immediate forcing term, then dynamic processes are too important to neglect. The problem of the coastal boundaries is mostly significant on shorter time scales, which justified the offline approach to SAL when longer time scales are considered. However, even when weekly mean values are considered, our model ocean retains large areas with correlation coefficients around 0.6 and below, especially at the coasts, in the North Atlantic, the equatorial Atlantic, and in the North Pacific (Figure 2b). In our OMCT run, p_B variability on time scales longer than one week is especially small in the North Atlantic, which is why correlations remain low in this area. Patterns of correlation similar to those shown in Figure 2b are obtained when only variations slower than around 4 days are considered. We hence deduce that, for an adequate representation of SAL effects faster than 4 days, online calculations during the model run are necessary. Slower variations can be sufficiently reproduced by offline corrections.

[25] Nevertheless, even if SAL has to be computed at every time step, there may be ways to reduce the computational complexity. Since the decomposition of the p'_B field into spherical harmonics is computationally expensive, just like the alternative of the field's convolution with the application of Green's Functions, the additional SAL potential term has often been computed as a multiplication of a scalar with the p'_B forcing field. This approach dates back to *Accad and Pekeris* [1978], who also calculated the value of 0.085 for the scalar factor β in equation (14). A comparable approach, although based on approximating p'_B with the simulated sea surface heights, has been included in an earlier version of OMCT [*Thomas et al.*, 2001]. The magnitude of β, however, depends very much on the specifications of the ocean model in use. This results from the degree-dependent terms $\alpha'_n\,(1 + k'_n - h'_n)$ in equation (13), which equal β if summed up.They decrease with increasing degree, thus high variability on smaller spatial scales leads to a smaller β value. The finer the model resolution, the smaller a value for β one would therefore expect, because smaller p_B anomalies can be resolved. We thus refrain from using the *Accad and Pekeris* [1978] value but compute a β appropriate to our OMCT configuration.

[26] The first way to achieve this is to describe the output of the SAL routine, i.e., the modification of the local potential due to SAL or the parenthesis in equation (13), as a function of the input, i.e., the local anomalies in ocean bottom pressure $p'_B(t)$. The slope of a straight line $V(t) = \beta \cdot p'_B(t)$ + const. fitted to these points serves as a temporal mean for β at a specific grid point. Its distribution is depicted in Figure 3a. A clear zonal dependency is obvious: Around the equator, β goes up to 0.2; in the northern and southern extratropics, values around 0.05 prevail. A similar distribution, although achieved with a very different ocean

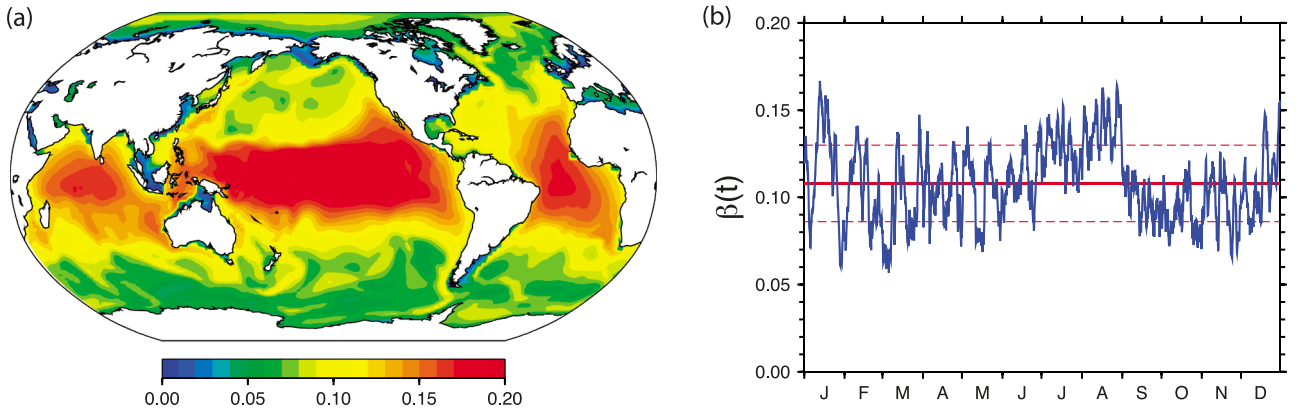

Figure 3. Optimal values for β as defined in equation (14) distributed in space and time. (a) We first described the modifications to the local potential due to self-attraction and loading $V(t)$ (the sum in equation (13)) as a function of the local anomalies in ocean bottom pressure $p'_B(t)$. We then fitted a straight line to this function $V(t) = \beta \cdot p'_B(t) + \text{const}$. For each grid point, β is the slope of this line. The area-weighted mean of the field is $\overline{\beta} = 0.100 \pm 0.072$. (b) The time series shows $\beta(t)$ as obtained by summing up degree-dependent expression $(1 + k'_n - h'_n)\rho\alpha'_n$ from equation (13), weighted by root-square sum of the Stokes coefficients calculated from the local anomalies in ocean bottom pressure $p'_B(t)$. The mean value of the time series is $\overline{\beta} = 0.108 \pm 0.022$, as indicated by the red lines.

model (OCCAM), has been obtained by *Stepanov and Hughes* [2004], who argued that smaller p'_B signals in the high latitudes caused by the more complex topography lead to this kind of distribution. The area-weighted mean of the field in Figure 3a is $\overline{\beta} = 0.100 \pm 0.072$.

[27] The second way of computing values for β is to take the Stokes coefficients a_{nm} and b_{nm} of the decomposition into orthonormal spherical harmonics that describes the p'_B field at every time step. With a_{nm} and b_{nm}, we quantify the power of the sine and cosine terms of degree n and order m. We compute $\beta(t)$ as the mean value of $\rho\alpha'_n(1 + k'_n - h'_n)$ for all degrees n weighted by the input field's power $\sum_m \sqrt{a_{nm}^2 + b_{nm}^2}$. The result is a value for β at every time step, shown in Figure 3b. We observe that the mean value $\overline{\beta} = 0.108 \pm 0.022$ is very close to what we obtained from the former way of computation. Furthermore, the spread of $\beta(t)$ around the mean value is as large as 20%. This, in combination with the large regional variability from Figure 3a, leads us to be skeptical of transferring the *Accad and Pekeris* [1978] parameterization, which postulates β to approximately be constant in space and time, from tidal models to circulation models. For tidal models, the *Accad and Pekeris* [1978] parameterization can be justified by assuming the dominance of one specific spatial scale in the p_B variations. This assumption only fails in regions close to the coast [*Ray*, 1998]. In circulation models, the multitude of spatial scales in p_B variations is apparently inconsistent with the assumption underlying the parameterization.

[28] Last, we want to quantify how large the errors are that we make assuming β to be constant anyway. This approach saves us from laboriously decomposing a global field into spherical harmonics and reassembling it at every time step, but instead offers a simple scalar multiplication. In accordance with our results from Figure 3, we choose a value of $\beta = 0.1$. We quantify the beta0.1 run's inaccuracy by first computing its differences to the Love run and then taking the standard deviation of these differences (Figure 4). To give an impression of the relative importance of these deviations, we also show contour lines describing this inaccuracy as a fraction of the total variability in the Love run. Figure 4 shows these error measures for the sea level relative to the ocean floor (Figure 4a), the absolute horizontal water velocity in the mixed layer (Figure 4b), and the water density modified by temperature and salinity in the same layer (Figure 4c), analogously to Figure 1.

[29] In Figure 4a, we see that the simulated sea level in the parameterized run in the tropical oceans is practically identical to the one computed with the full SAL formulation. In the northern and southern extratropical open oceans, errors are around 0.2 cm; in certain parts of the ACC, they attain 0.4 cm. These errors make out around 5% of the total sea level signal. Only in certain coastal waters (e.g., Gulf of Thailand, East China Sea, Barents Sea, North Sea), where dynamics are strong and OMCT modeling is arguably weak, errors reach 0.8 cm. Comparing these results with Figure 1a, we see that the errors in sea level resulting from neglecting SAL can easily be halved by a parameterization like that of *Accad and Pekeris* [1978].

[30] The picture is different for velocities (Figure 4b) and density (Figure 4c). Here, errors made by the beta0.1 run are just as large as if SAL had been omitted in the first place. As explained above, SAL impacts on these two variables are small in absolute values; but if one wishes to consider these impacts anyway, the errors caused by the scalar approximation are too large, reaching up to 0.1 cm/s in velocity and 0.01 kg/m^3 in density. The regional distribution in Figures 4b and 4c also shows that there are no regions where a scalar SAL approximation, omitting remote effects, does a particularly good job. As a result, we conclude that a simple parameterization can be of use to improve simulated sea levels, but neither currents nor density distributions.

5. Summary

[31] We provide a theoretical description for incorporating the variations of the local potential due to self-attraction and

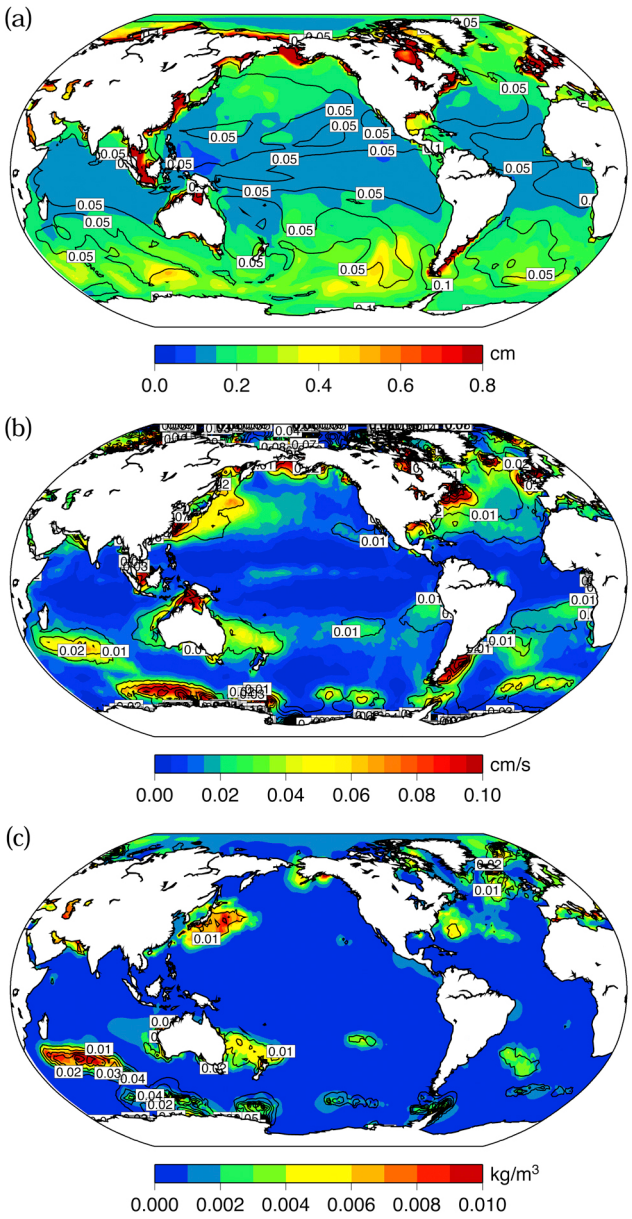

Figure 4. Error in (a) relative sea level, (b) absolute horizontal velocity in the upper 90 m, and (c) water density in the upper 90 m caused by using a parameterization instead of the full formulation to describe SAL effects. Colors show the absolute error made in terms of the standard deviation of differences between the Love run and the beta0.1 run. Black contour lines show the relative error caused by the parameterization in terms of the former quantity divided by the standard deviation of the Love run.

loading (SAL) into a global baroclinic ocean model. After implementing this routine into the OMCT model, we analyzed three 1 year simulations: One with SAL considered in the theoretically most complete way (Love), one with SAL parameterized following *Accad and Pekeris* [1978] (beta0.1), and one with SAL switched off (noSAL). We show that, for an accurate representation of SAL, it needs to be calculated during the model run, and not only as a postprocessing correction to sea levels. We then go on to show that omitting SAL completely results in errors reaching between 0.6 and 0.8 cm in relative sea level close to the coasts. This is equivalent to a mean error of around 10% in relative sea level predictions. In the open ocean, these errors mostly remain around 0.3 cm. Feedbacks on horizontal velocities and density are apparent but rather small. Considering a scalar approximation to SAL, as proposed by *Accad and Pekeris* [1978], we compute an optimal value of the scalar factor β which turns out to be 0.1 for our ocean model. However, large variabilities of β in space and time, as well as the incapability of the parameterization to meaningfully reproduce SAL effects except for the direct effect on sea level, lead us to reject this approach.

6. Conclusions

[32] 1. A full consideration of SAL effects in a serial baroclinic ocean model is feasible, although the additional computing time at every time step has to be weighed against the expected improvement of the simulations. In the case of OMCT, computing time increases by around 16%.

[33] 2. Correcting for SAL in the postprocessing seems promising as it saves a lot of computing time. The OMCT, for instance, works with a time step of 30 min, while the output fields are only written every 6 h. However, these postprocessing or offline approaches fail to grasp all dynamical feedbacks and all impacts on hydrographic variables. Even for sea level, the possible offline corrections seem doubtful in light of the low correlations between SAL forcing and response we observed on short time scales. For slower variations (>4 days), offline corrections of sea level are sufficient.

[34] 3. Offline corrections are, however, appropriate when time scales are long enough for the ocean to adapt to the new geoid. Since dynamic and baroclinic SAL effects are small, their omission by an offline correction can be justified.

[35] 4. SAL is an effect significant enough to be considered in OGCMs if we attempt to make errors smaller than 20% in sea level or smaller than 5% in horizontal velocity and density simulations, at least on subweekly time scales.

[36] 5. Scalar approximations to SAL are inappropriate since they neglect the strong spatial and temporal variability of bottom pressure spatial scales, which determine the scalar factor.

7. Outlook

[37] What remains to be done until SAL effects are satisfyingly represented in OGCMs? To employ the complete formulation, decomposing the global field of ocean bottom pressure anomalies into spherical harmonics at every time step, increases the computing time in the case of OMCT by around 16%; for parallelized models, the price would even be higher. Our implementation of SAL may therefore be useful when the focus lies on high-frequency sea level variability. When seasonal or interannual time scales are concerned, however, offline corrections are sufficient. The decomposition into spherical harmonics is especially computing time intensive for models of higher spatial and temporal resolution than OMCT. Therefore, better approx-

imations to the complete formulation, exceeding the scalar approximation in complexity, are desirable. The implementation we came up with can serve as a benchmark for such future approximations. Yet in light of the high frequencies at which nonlinear SAL effects are influential, approximations should not compromise the temporal or spatial resolution of the correcting field. Parameterizations based on latitude, ocean depth, or similar indicators may perform well in some cases [see, e.g., *Stepanov and Hughes*, 2004], but they lack a sound physical basis that would make them trustworthy without having to test them in each future modeling application.

[38] Another exercise for our model routine, especially once computational efficiency is improved, could be to simulate other sources of high-frequency potential deformation. Examples may be rapid changes in land hydrology or possible interactions between tidal variations and ocean circulation. While in this study we focused on nontidal ocean loadings, the OMCT also contains an ephemeral tidal model, and our SAL-permitting configuration might be a means to explore this interaction between tides and circulation.

References

Abramowitz, M., and I. A. Stegun (1972), *Handbook of Mathematical Functions*, 470 pp., U.S. Dep. of Comm., Washington, D. C.

Accad, Y., and C. L. Pekeris (1978), Solution of the tidal equations for the M_2 and S_2 tides in the world oceans from a knowledge of the tidal potential alone, *Philos. Trans. R. Soc. A*, *290*(1368), 235–266, doi:10.1098/rsta.1978.0083.

Bindoff, N., et al. (2007), Observations: Oceanic climate change and sea level, in *Climate Change 2007: The Physical Science Basis. Contribution of Working Group I to the Fourth Assessment Report of the Intergovernmental Panel on Climate Change*, edited by S. Solomon et al., pp. 385–432, Cambridge Univ. Press, Cambridge, U. K.

Blewitt, G. (2007), *Treatise on Geophysics*, vol. 3, *Geodesy*, 446 pp., Elsevier, Amsterdam.

Cazenave, A., K. Dominh, S. Guinehut, E. Berthier, W. Llovel, G. Ramillien, M. Ablain, and G. Larnicol (2009), Sea level budget over 2003–2008: A reevaluation from GRACE space gravimetry, satellite altimetry and Argo, *Global Planet. Change*, *65*, 83–88, doi:10.1016/j.gloplacha.2008.10.004.

Chambers, D. P., and J. K. Willis (2010), A global evaluation of ocean bottom pressure from GRACE, OMCT, and steric-corrected altimetry, *J. Atmos. Oceanic Technol.*, *27*, 1395–1402, doi:10.1175/2010JTECHO738.1.

Church, J. A., and N. J. White (2006), A 20th century acceleration in global sea-level rise, *Geophys. Res. Lett.*, *33*, L01602, doi:10.1029/2005GL024826.

Dee, D. P., et al. (2011), The ERA-Interim reanalysis: Configuration and performance of the data assimilation system, *Philos. Trans. R. Soc. A*, *137*(656), 553–597, doi:10.1002/qj.828.

Dill, R. (2008), Hydrological model LSDM for operational Earth rotation and gravity field variations, *Tech. Rep. STR 08/09*, 35 pp., GFZ Ger. Res. Cent. for Geosci., Potsdam, doi:10.2312/GFZ.b103-08095.

Dobslaw, H., R. Dill, A. Grötzsch, A. Brzeziński, and M. Thomas (2010), Seasonal polar motion excitation from numerical models of atmosphere, ocean, and continental hydrosphere, *J. Geophys. Res.*, *115*, B10406, doi:10.1029/2009JB007127.

Drijfhout, S., C. Heinze, M. Latif, and E. Maier-Reimer (1996), Mean circulation and internal variability in an ocean primitive equation model, *J. Phys. Oceanogr.*, *26*, 559–580.

Dziewonski, A. M., and D. L. Anderson (1981), Preliminary reference Earth model, *Phys. Earth Planet. Inter.*, *25*, 297–356.

Farrell, W. E. (1973), Earth tides, ocean tides and tidal loading, *Philos. Trans. R. Soc. London, Ser. A*, *274*, 253–259, doi:10.1098/rsta.1973.0050.

Flechtner, F. (2007), GFZ level-2 processing standards document, 19 pp., technical report, GFZ Potsdam, Potsdam, Germany. [Available at http://isdc.gfz-potsdam.de/index.php?name=UpDownload&req=getit&lid=401.]

Greatbatch, R. J. (1994), A note on the representation of steric sea level in models that conserve volume rather than mass, *J. Geophys. Res.*, *99*(C6), 12,767–12,771, doi:10.1029/94JC00847.

Meehl, G., et al. (2007), Global climate projections, in *Climate Change 2007: The Physical Science Basis. Contribution of Working Group I to the Fourth Assessment Report of the Intergovernmental Panel on Climate Change*, edited by S. Solomon et al., pp. 747–845, Cambridge Univ. Press, Cambridge, U. K.

Müller, M. (2007), A large spectrum of free oscillations of the World Ocean including the full ocean loading and self-attraction effects, Ph.D. thesis, 103 pp., Univ. Hamburg, Hamburg, Germany, doi:10.1007/978-3-540-85576-7.

Munk, W., and G. J. F. MacDonald (1960), *The Rotation of the Earth—A Geophysical Discussion*, 323 pp., Cambridge Univ. Press, Cambridge, U. K.

Oliver, E., and K. Thompson (2010), Madden-Julian Oscillation and sea level: Local and remote forcing, *J. Geophys. Res.*, *115*, C01003, doi:10.1029/2009JC005337.

Quinn, K. J., and R. M. Ponte (2011), Estimating high frequency ocean bottom pressure variability, *Geophys. Res. Lett.*, *38*, L08611, doi:10.1029/2010GL046537.

Ray, R. D. (1998), Ocean self-attraction and loading in numerical tidal models, *Mar. Geod.*, *21*, 181–192, doi:10.1080/01490419809388134.

Smirnow, W. I. (1955), *Lehrgang der Höheren Mathematik Teil III/2*, 601 pp., Dtsch. Verlag der Wissenschaften, Berlin.

Stepanov, V. N., and C. W. Hughes (2004), Parameterization of ocean self-attraction and loading in numerical models of the ocean circulation, *J. Geophys. Res.*, *109*, C03037, doi:10.1029/2003JC002034.

Tamisiea, M. E., E. M. Hill, R. M. Ponte, J. L. Davis, I. Velicogna, and N. T. Vinogradova (2010), Impact of self-attraction and loading on the annual cycle in sea level, *J. Geophys. Res.*, *115*, C07004, doi:10.1029/2009JC005687.

Thomas, M. (2002), Ozeanisch induzierte Erdrotationsschwankungen: Ergebnisse eines Simultanmodells für Zirkulation und ephemeridische Gezeiten im Weltozean, Ph.D. thesis, 128 pp., Univ. Hamburg, Hamburg, Germany.

Thomas, M., J. Sündermann, and E. Maier-Reimer (2001), Consideration of ocean tides in an OGCM and impacts on subseasonal to decadal polar motion excitation, *Geophys. Res. Lett.*, *28*, 2457–2460.

Thompson, K., and E. Demirov (2006), Skewness of sea level variability of the world's oceans, *J. Geophys. Res.*, *111*, C05005, doi:10.1029/2004JC002839.

Vinogradova, N. T., R. M. Ponte, M. E. Tamisiea, J. L. Davis, and E. M. Hill (2010), Effects of self-attraction and loading on annual variations of ocean bottom pressure, *J. Geophys. Res.*, *115*, C06025, doi:10.1029/2009JC005783.

Vinogradova, N. T., R. M. Ponte, M. E. Tamisiea, K. J. Quinn, E. M. Hill, and J. L. Davis (2011), Self-attraction and loading effects on ocean mass redistribution at monthly and longer time scales, *J. Geophys. Res.*, *116*, C08041, doi:10.1029/2011JC007037.

Wolff, J.-O., E. Maier-Reimer, and S. Legutke (1996), The Hamburg Ocean Primitive Equation Model, *Tech. Rep. 13*, 110 pp, Dtsch. Klimarechenzent., Hamburg, Germany.

Wunsch, C., R. M. Ponte, and P. Heimbach (2007), Decadal trends in sea level patterns: 1993–2004, *J. Clim.*, *20*, 5889–5911, doi:10.1175/2007JCLI1840.1.

Yin, J., S. M. Griffies, and R. Stouffer (2010), Spatial variability of sea level rise in twenty-first century projections, *J. Clim.*, *23*, 4585–4607, doi:10.1175/2010JCLI3533.1.

H. Dobslaw, J. Kuhlmann, and M. Thomas, Section 1.3: Earth System Modelling, GFZ German Research Centre for Geosciences, Telegrafenberg, D-14473 Potsdam, Germany. (julian.kuhlmann@gfz-potsdam.de)